metals

MDPI

Article

Research on Fatigue Strength for Weld Structure Details of Deck with U-rib and Diaphragm in Orthotropic Steel Bridge Deck

Yixin Chen *, Pengmin Lv and Datao Li

Key Laboratory of Road Construction Technology & Equipment, Ministry of Education, Chang'an University, Xi'an 710064, China; lpmin@chd.edu.cn (P.L.); ldt1688@chd.edu.cn (D.L.)

* Correspondence: chenyx@chd.edu.cn; Tel.:+86-29-82334586

Received: 3 April 2019; Accepted: 23 April 2019; Published: 26 April 2019

Abstract: The orthotropic steel bridge deck weld structure would easily cause fatigue cracking under the repeated action of vehicle load. This paper took the steel box girder in a bridge as a research object, researched the mechanical properties of the steel plate and the microstructure of the welded joint, then designed the fatigue specimens of the deck plate and did the fatigue test. The $\Delta\sigma$-N curves and stress amplitudes of the weld details of the deck plate with U-rib and diaphragm under different probabilities of survival were obtained. After extended the $\Delta\sigma$-N curves to the long life range, the fatigue damage calculation equation of the detail was proposed, and the cut-off limit under the 50% and 97.7% probability of survival were 81.50 MPa and 53.11 MPa, respectively. Based on the actual vehicle load spectrum and simplified finite element model of the steel box girder section, the stress amplitude of the details of the weld joint was calculated. The calculation result shows that the maximum stress amplitude of the concerned point was 38.29 MPa, less than the cut-off limit. It means that the fatigue strength of the details of the weld joint meet the requirement of the fatigue design.

Keywords: orthotropic steel bridge deck; weld joint; fatigue design curve; fatigue strength; fatigue test

1. Introduction

Due to the advantages such as a light weight, guarantee of high quality, convenience for in-situ assembling process, etc., the orthotropic steel decks have become very frequently used in the construction of bridges [1–3]. The orthotropic steel bridge deck is a steel deck system with longitudinal ribs and floor beams to support and resist the applied loads such as vehicles and the dead load, and transfer these loads to the main bridge system, which has different types of structures and stiffness values in the longitudinal and transverse directions [4,5]. Much study has shown that the fatigue failure was one of the major factors in the failure of steel bridges [6–9], and which is liable to fatigue cracking once placed in service [10]. Fatigue cracks originated in welded details of the orthotropic steel bridge deck, which greatly impacted on the traffic safety and limited the service life, especially in deck-to-rib joints [11,12]. Under the action of a moving wheel, the damage on the deck plate can highly increase the displacement and stress level of the weld detail because of the changes in its structural behaviors and response generated from the longitudinal ribs against moving loads in the longitudinal direction [13]. It was local stress concentration caused by interaction between out-of-plane motion of U-ribs to adjacent cross-beams and in-plane distortion of the cross-beam that induces the secondary stresses, which may initiate fatigue cracks inside the cross-beams [14]. In addition, there are local stress concentrations on the components caused by residual stresses and weld defects in the weld details, and the geometric abrupt changes at the weld defects and the initial defects of the weld details, which will accelerate the local fatigue crack initiation and expansion [15,16]. Connor and

Fisher researched on fatigue resistance of the weld details, and presented a procedure to calculate the stresses at the rib-to-diaphragm joint [17]. Maljaars et al. developed a linear elastic fracture mechanics model for the typical fatigue crack that observed at the root of the weld between the deck plate and stringer [18]. Xiao et al. used the finite element software to study stress analyses and fatigue evaluation of rib-to-deck joints in steel orthotropic decks [19]. Kainuma et al. investigated the fatigue behaviors of the rib-to-deck welded joints and the results showed that the root gap shape and penetration rate have an impact on the root cracking direction and fatigue life [20,21]. Heng et al. evaluated the fatigue performance of rib to deck welded joints in orthotropic steel decks with thickened edge U-ribs, and compared the fatigue performance with the specimens that have conventional U-ribs [22]. Yu et al. did the fatigue test on the typical weld structural details of a steel bridge deck, and the results showed that the cracks tend to occur at the weld locations of the ends and longitudinal ribs and in the bridge deck plate outside the longitudinal ribs [23]. Luo et al. evaluated the fatigue strength of rib-to-deck weld joint in orthotropic steel deck by an average strain energy density method, and derived a W-N curve for the fatigue evaluations [24]. The actual engineering inspection showed that the roof and stiffener welds are most likely to fatigue crack when they are located at the intersection of the diaphragm [25].

However, the stress distribution of the deck plate at its weld joints with U-rib and diaphragm is complicated. The crack is easily initiated in this structural detail, but there are relatively few studies on fatigue behaviors of this detail. In order to make sure the bridge can be working safely, it is necessary to deeply research the fatigue behaviors of the structural detail.

In this paper, the research on the mechanical properties and the microstructure of the steel plate at the welded joint with U-rib and diaphragm were carried out, and then the specimens of the deck plate were designed for the fatigue test. According to the results, the $\Delta\sigma$-N curve and the fatigue damage calculation equation that meets the requirement of the fatigue design of the detail are proposed. This paper also established a simplified finite element model of the steel box girder section, and calculated the stress amplitude of the details of the weld joint using the actual vehicle load spectrum. The calculation result shows that the maximum stress amplitude of the concerned point was less than the cut-off limit.

2. Fatigue Test for Weld Structure of U-Rib and Deck Plate

In order to study the mechanical properties of Q345qD steel plates, a tensile test was carried out using a SD-500 fatigue test machine. Three specimens were designed according to International Standard ISO 6892-1 [26].

According to the standards TB 10002.2-2005 [27] and GB/T 10045-2001 [28], the chemical compositions of Q345qD and the welding wire E501T-1 are shown in Table 1. The test results of the yield strength and the tensile strength are shown in Table 2.

Table 1. The chemical compositions of Q345qD and the welding wire.

Designation	Element (%)					
	C	Si	Mn	P	S	Als
Q345qD	≤0.18	≤0.60	1.1–1.6	≤0.025	≤0.025	≥0.015
E501T-1	≤0.18	≤0.90	≤1.75	≤0.03	≤0.03	-

Table 2. The mechanics performance of Q345qD and the welding wire.

Designation	Specimen Number	Yield Strength/MPa	Tensile Strength/MPa
Q345qD	1	331.3	507.5
	2	342.6	517.3
	3	344.5	509.9
	Mean value	339.5	511.6
E501T-1	1	495	575

2.1. Microstructure Analysis of Welded Joint

The microstructure of the welded joint is different in base metal, weld metal, and the heat affected zone. The local weld joint of the sample was dissected and the sample was corroded in 4% nitric acid alcohol solution for 10 s.

Figure 1a shows the microstructures of the steel specimen, the steel specimen had a ferrite and pearlite banded structure. Figure 1b shows the microstructures of the welded joint, the ferrite was distributed along the columnar crystal on the matrix of sorbite. When the weld was cooled down, the molten metal in the weld was crystallized along the direction of the thermal diffusion, and the columnar crystal was obtained. The eutectoid ferrite separated out along the columnar crystal first, and this ferrite was slightly overheated as the temperature was higher and the cooling rate was slightly faster. During the subsequent cooling process, the austenite turned into acicular distribution of sorbite as greater under-cooling. Figure 1c shows the microstructures of the heat affected zone, and this zone was mainly sorbite and reticular or an acicular distribution of ferrite on the matrix of the Widmanstätten structure.

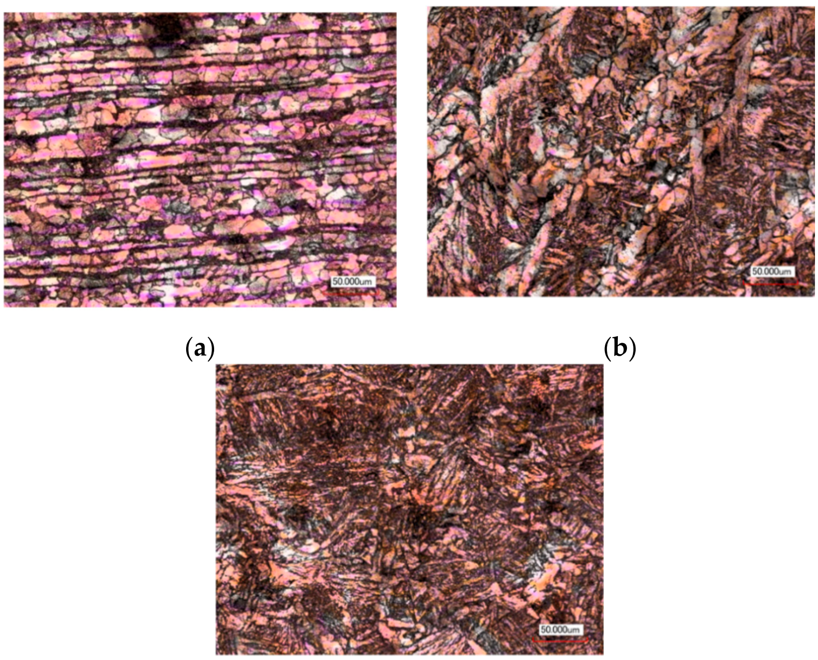

(**a**) (**b**) (**c**)

Figure 1. Microstructures of a steel weld joint: (**a**) Steel specimen; (**b**) weld metal; and (**c**) the heat affected zone.

Due to the uneven distribution of the microstructure in the weld area, different degrees of grain coarsening appeared in the fusion zone, which is the weak area of the whole welded joint. The property of the fusion zone was also uneven, which affects the mechanical properties, corrosion resistance, and fatigue resistance of the joint.

2.2. Fatigue Test and Result Analysis

The fatigue specimens were designed and fabricated via V-groove welding. The welding procedure of the specimen was the same as that in the real bridge, which adopted the carbon dioxide arc welding method and used a six-pass welding process. The specific welding parameters are shown in Table 3.

Table 3. Welding parameters.

Electrode Diameter (mm)	Welding Current (A)	Arc Voltage (V)	Welding Speed (cm/min)
Φ1.2	180	24	20

The fatigue test was done by a SD-500 fatigue test machine (produced by Sinotest Equipment Co. ltd, Changchun, China). The stress ratio was set as $R = 0.05$ in the fatigue test. Eleven groups of the fatigue test results were shown in Table 4. Among these eleven specimens, the surface of the specimen sy-2-1-2 and sy-2-1-6 were polished and smoothed to research the influence of surface roughness on fatigue life.

Table 4. Fatigue test results of eleven specimens.

Specimens Number	Stress Amplitudes $\Delta\sigma$/MPa	Number of Cycles N	lg$\Delta\sigma$	lg$N$
SY-2-1-1	332.4	152,168	2.522	5.182
SY-2-1-2	272.4	820,188	2.435	5.914
SY-2-1-3	212.5	1,031,746	2.327	6.014
SY-2-1-4	164.5	1,513,565	2.216	6.180
SY-2-1-5	272.4	365,118	2.435	5.562
SY-2-1-6	272.4	1,354,662	2.435	6.132
SY-2-1-7	272.4	290,476	2.435	5.463
SY-2-1-8	272.4	376,123	2.435	5.575
SY-2-1-9	272.4	217,132	2.435	5.337
SY-2-1-10	272.4	677,876	2.435	5.831
SY-2-1-11	176.5	1,419,414	2.247	6.152

According to the data shown in Table 4, the $\Delta\sigma$-N curve equation at 50% probability of survival of the details of the structure was fitted as shown in Equation (1):

$$\lg N = 14.965 - 3.876 \lg \Delta\sigma, \tag{1}$$

where, $\Delta\sigma$ is the stress amplitude, N is the number of cycles corresponding to failure. When $N = 2 \times 10^6$, $\Delta\sigma_1$ was equal to 171.92 MPa.

$\Delta\sigma$-N curve equations and stress amplitudes for different probabilities of survival of the structure details were calculated based on Equation (1), as shown in Table 5. The $\Delta\sigma$-N curve equations and stress amplitudes for different probabilities are shown in Figure 2.

Table 5. $\Delta\sigma$-N curve equations and stress amplitude for different failure probabilities.

Probabilities of Survival (%)	$\Delta\sigma$-N Curve Equations	Stress Amplitude $\Delta\sigma$/MPa ($N = 2 \times 10^6$)
60	$\lg N = 14.875 - 3.876\lg\Delta\sigma$	162.95
70	$\lg N = 14.778 - 3.876\lg\Delta\sigma$	153.81
80	$\lg N = 14.663 - 3.876\lg\Delta\sigma$	143.64
90	$\lg N = 14.504 - 3.876\lg\Delta\sigma$	130.74
97.7	$\lg N = 14.244 - 3.876\lg\Delta\sigma$	112.08
99	$\lg N = 14.126 - 3.876\lg\Delta\sigma$	104.44

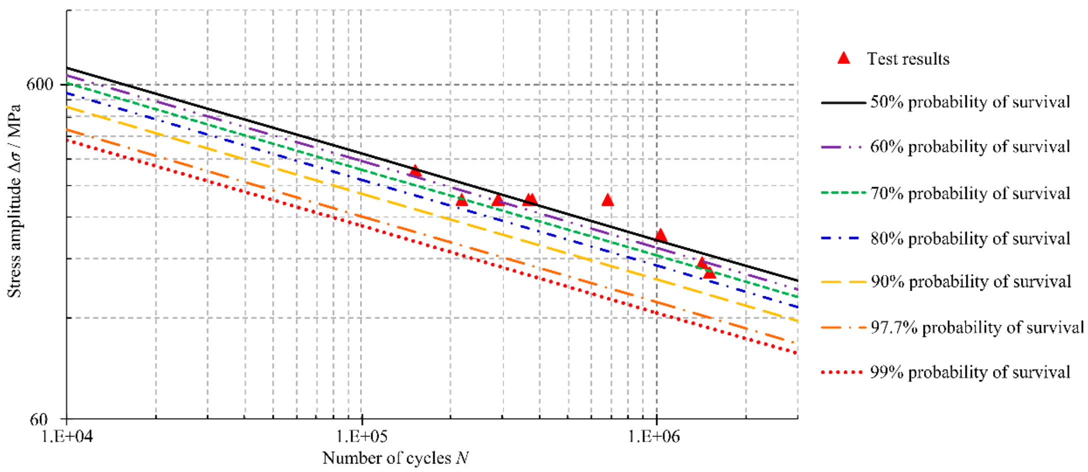

Figure 2. The curves of $\Delta\sigma$-N.

The crack propagation has been monitored by electron microscopy, as shown in Figure 3. According to the fatigue test, the initial crack occurred at the base metal of the bridge deck surface at its welded joint with the diaphragm and U-rib, and then extended lengthwise along the U-rib. The crack location, extension direction, and local view are shown in Figure 3. The crack occurred at the top surface of the bridge deck and was affected by the weld, so the fatigue strength of the details was lower than the base metal, but higher than the weld.

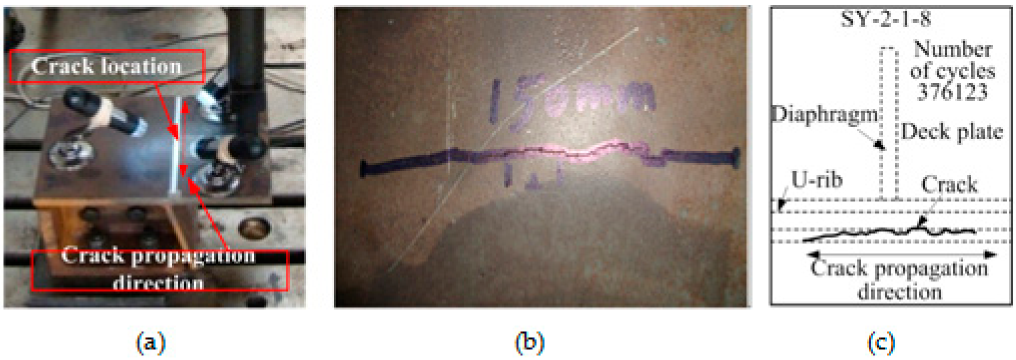

Figure 3. The crack of the specimen SY-2-1-8: (**a**) Fatigue test; (**b**) crack of the specimen; and (**c**) the position of the crack.

Named the number of cycles when the initial crack occurred as N_1, then compared N_1 with the number of cycles N when the specimen was fractured, and the proportion of initiation life could be obtained, as shown in Table 6.

According to the data shown in Table 6, the $\Delta\sigma$-N_1 curve equation at 50% probability of survival of the details of the structure was fitted as shown in Equation (2):

$$\lg N_1 = 15.717 - 4.219\lg\Delta\sigma, \tag{2}$$

when $N = 2 \times 10^6$, $\Delta\sigma_2$ was equal to 170.47 MPa.

The $\Delta\sigma$-N_1 curve equation at 97.7% probability of survival of the details of the structure was fitted as shown in Equation (3):

$$\lg N_1 = 14.939 - 4.219\lg\Delta\sigma, \tag{3}$$

when $N = 2 \times 10^6$, $\Delta\sigma_2$ was equal to 111.53 MPa.

From Table 6 and Figure 4, it could be easily seen that the initiation life of the crack in the weld detail was longer than the crack propagation life.

Table 6. The proportion of initiation life for each specimen.

Specimen Number	Stress Amplitude $\Delta\sigma$/MPa	Number of Cycles when Crack Occurred N_1	Number of Cycles N	Proportion of Initiation Life
SY-2-1-1	332.37	113,210	152,168	74.40%
SY-2-1-3	212.47	964,524	1,031,746	93.48%
SY-2-1-4	164.51	1,440,870	1,513,565	95.20%
SY-2-1-5	272.42	323,484	365,118	88.60%
SY-2-1-7	272.42	230,748	290,476	79.44%
SY-2-1-8	272.42	351,444	376,123	93.44%
SY-2-1-9	272.42	171,784	217,132	79.12%
SY-2-1-10	272.42	592,622	677,876	87.42%
SY-2-1-11	176.50	1,207,128	1,419,414	85.04%

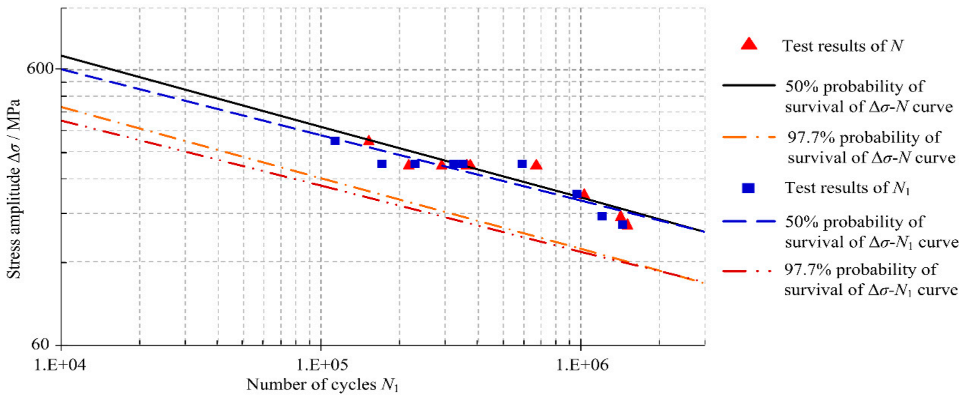

Figure 4. The comparison between the curves $\Delta\sigma$-N and $\Delta\sigma$-N_1.

2.3. The Effect of Surface Roughness on Fatigue Life

According to the principle of fracture mechanics, the larger the surface roughness, the larger the stress concentration coefficient, and leads to a worse fatigue performance.

In order to study the effect of surface roughness on the fatigue life of weld structure of U-rib and deck plate, the surface of the specimen sy-2-1-2 and sy-2-1-6 were smoothed, and the comparison was conducted during the fatigue test. The test results showed that the fatigue life would be improved significantly when the surface of the specimen was polished. The crack location, extension direction, and local view are shown in Figure 5. The number of cycles of the specimen sy-2-1-2 and sy-2-1-6 were calculated by Equation (1) to obtain the theoretical number of cycles. The comparison between the theoretical number of cycles and the test number of cycles is shown in Table 7. The life expectancy rate of the specimen sy-2-1-2 was about 138.2%, and the life-expectancy rate of the specimen sy-2-1-6 was 293.4%.

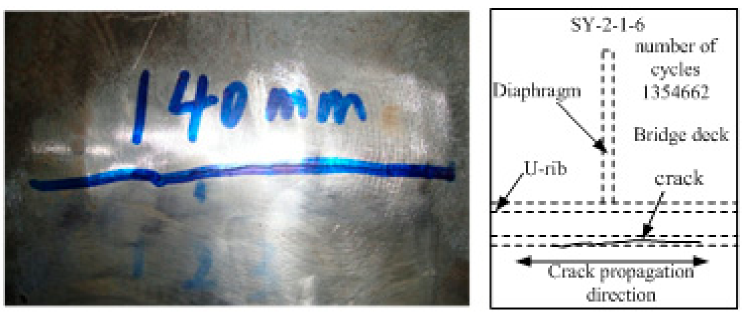

(a) (b)

Figure 5. The crack of the specimen SY-2-1-6: (**a**) Crack of the specimen; and (**b**) position of the crack.

Table 7. The comparison between theoretical number of cycles and test number of cycles.

Specimen Number	Theoretical Number of Cycles	Test Number of Cycles	Growth Rate/%
SY-2-1-2	344,372	820,188	138.2%
SY-2-1-6	344,372	1,354,662	293.4%

3. Stress Spectrum Calculation

The fatigue life of the steel bridge deck is related to the stress amplitude and the number of cycles under the action of vehicle load. The calculation of stress amplitude spectrum is important for the fatigue design of steel bridge deck. In order to analyze the stress condition of the deck plate at its weld joint with U-rib and diaphragm, the simplified finite element model of steel bridge was established. The vehicle load spectrum was calculated based on the actual vehicle survey data, and the stress-time history of the concerned point under vehicle load was calculated, then the stress spectrums were obtained by the rain flow counting method.

3.1. Loading Method

According to the actual vehicle survey data, the load frequency spectrum of vehicle load for a certain bridge was obtained. The passing vehicles were divided into seven types on the basis of vehicle type, number of axles, wheelbase, and vehicle weight, as shown in Table 8. The values of lane distribution coefficient were shown in Tables 9 and 10 [29]. The loading method in this paper is single lane loading.

Table 8. Vehicle load frequency spectrum for the certain bridge (96 h).

Vehicle Model	Number of Axles	Illustrations Axle Load/kN, Wheelbase/mm	Total Weight/kN	Number of Vehicles	Ratio of Total Traffic
V1	2	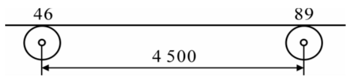	137	19,078	14.74%
V2	3	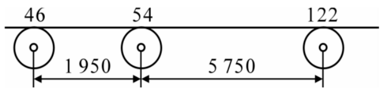	222	2778	2.15%
V3	3	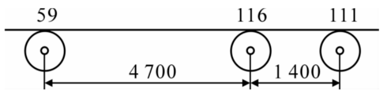	318	916	0.71%
V4	4	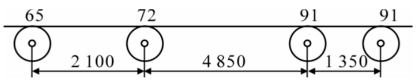	317	5342	4.13%
V5	5	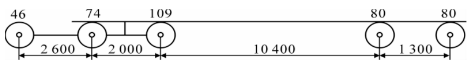	375	163	0.13%
V6	5	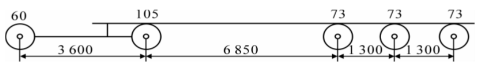	384	1682	1.30%
V7	6	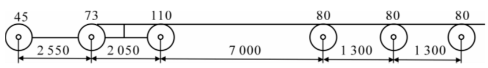	467	18,009	13.91%
		Total		47,968	37.06%

Note: The front axle of vehicle had two tires, and the contact area between the wheel and the ground on each side was 0.3 m × 0.2 m. The other axles had four tires, and the contact area on each side was 0.6 m × 0.2 m. The wheel-track of the vehicle was 1.8 m.

Table 9. Lane distribution coefficient of two-axle vehicles.

Vehicle Weight	Vehicle Model	Inside Lane	Center Lane	Outside Lane
0–2 t	Cars, light buses	0.699	0.248	0.054
2–8 t	Bus Two axle truck I	0.244	0.372	0.384
>8 t	Two-axle bus Two axle truck II	0.042	0.650	0.309

Table 10. Lane distribution coefficient of multi-axle vehicles.

Number of Axles	Daily Average Number of Vehicles	Inside Lane	Center Lane	Outside Lane
3	1171	0.076	0.435	0.489
4	3384	0.043	0.310	0.648
5	1284	0.067	0.401	0.533
6	543	0.091	0.420	0.488

3.2. FE Model and Stress Calculation of Steel Bridge Structure

3.2.1. Simplified Finite Element Model of Steel Bridge Structure

The target bridge is designed for six lane highways, which has a main bridge length of 140,500 mm and a main span of 81,800 mm. The length of each side span is 22,900 and 35,800 mm, respectively. The bridge structure layout is shown in Figure 6.

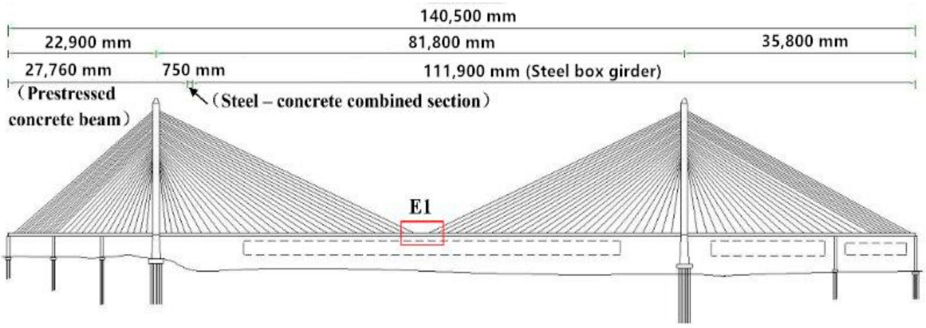

Figure 6. The bridge structure layout.

In this paper, the steel box girder section with the maximum stress variation under the vehicle load was selected as the research object, and named E1. The length of this steel girder section was 15 m, the thickness of the deck plate was 16 mm, the cross section of the longitudinal rib was 300 mm (top width) × 180 mm (bottom width) × 300 mm (height), and the thickness of the rib was 8 mm. The space between two U-ribs was 0.6 m and the space between two diaphragms was 3.75 m. The thickness of the diaphragms was 12 mm and 14 mm, respectively.

Due to the centrosymmetric structure of the steel box girder section, the one-fourth finite element model was established as shown in Figure 7. Based on the St. Venant principle, the simplified finite element model of the steel box girder section was established, as shown in Figure 8. The longitudinal length of the model was 11.25 m (3.75 m × 3 m) and the transverse length of the model was 4.8 m (0.6 m × 8 m). The elastic modulus of steel plate was 210 GPa and the Poisson's ratio was 0.3.

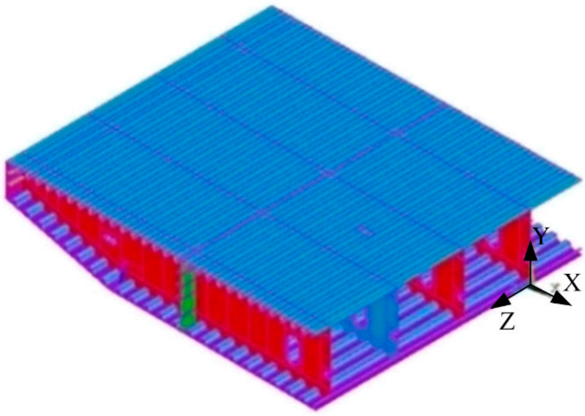

Figure 7. One-fourth finite element model of steel box girder section.

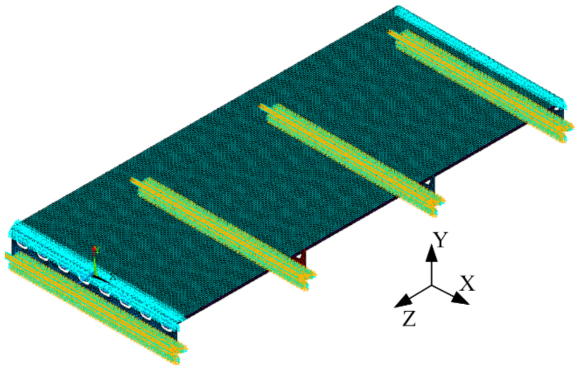

Figure 8. Simplified finite element model of steel box girder section.

Two assumptions were made in the finite element analysis as follows: (1) The components are made of homogeneous, continuous, and isotropic pure elastic materials, and (2) the self-weight and damping of the steel bridge deck are not considered.

Since the box girder webs could restrain the vertical deflection of the deck plate effectively, as shown in Figure 8, along the longitudinal direction (Z-axis) of the girder section, the vertical translation (along Y-axis) of one end of the section was constrained, and the vertical translation and the lateral displacement (along X-axis) of the other end were constrained. All six degrees of freedom of the diaphragms were fixed at the bottom.

3.2.2. Determination of the Concerned Point

The concerned point was located on the top surface of the deck plate at its weld joints with U-rib and diaphragm, as shown in Figure 9. In this position, the U-rib crossed through the perforated diaphragm and connected with the diaphragm by filled welds, and the stress concentration would exist at the perforated position of the diaphragm and the end of the welds. This position would be affected by the in-plane bending stress and the out-of-plane bending stress, which were caused by the deflection of the U-rib. Therefore, the fatigue cracks were easily generated at this concerned point of the deck plate under the action of the changing load of the vehicle.

When the vehicle load acting on the orthotropic steel bridge deck, there was a large stress value in the position of the load and its vicinity, but the stress value away from the load position was very small and the influence distance was much smaller than the vehicle wheelbase. Therefore, when analyzing the worst loading position of the bridge deck, it could use the dual-wheel load of the vehicle [16]. In order to get the worst loading position of the concerned point, take the vehicle model V2 in Table 9 as an example, the stress-time history curve was calculated based on the axle weight of one side of rear axle. The stress-time history curve and the worst loading position of the concerned point are shown in Figures 10 and 11, respectively.

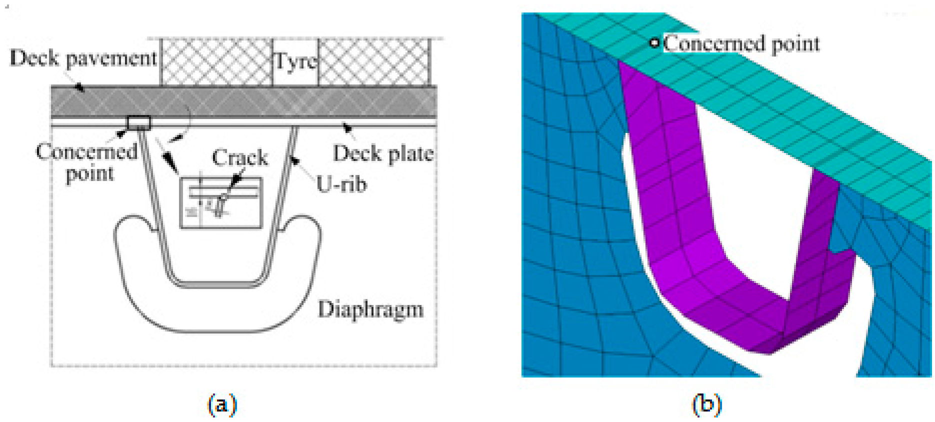

Figure 9. The position of the concerned point: (**a**) Position of the concerned point; and (**b**) the concerned point in the model.

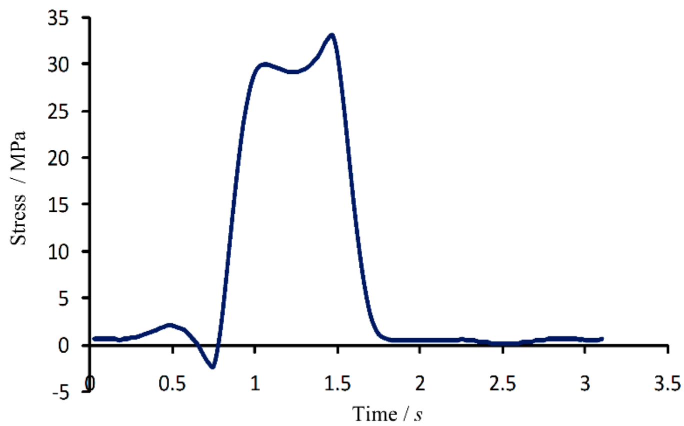

Figure 10. The stress-time curve of concerned point.

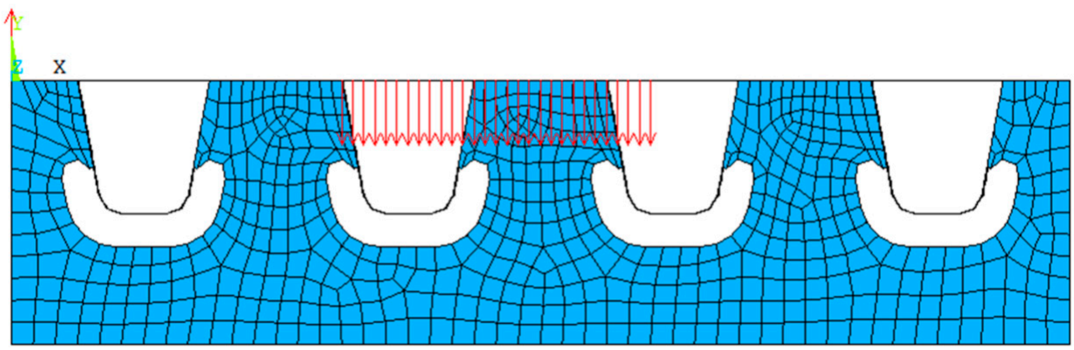

Figure 11. The worst loading position of the concerned point.

3.2.3. The Calculation of Stress Frequency Spectrum

The stress calculated by elastic theory should be included in the impact effect of the vehicle load. According to AASHTO LRFD Bridge Design Specifications [30], the impact coefficient was adopted to be 0.15 in this paper.

Due to the influence of the deck pavement on the contact area between the wheel and the ground, the wheel load was extended to the bridge deck along the 45° direction during the loading process.

Thus, the contact area of the front wheel should be modified to 0.41 m × 0.31 m and the modified contact areas of the remaining wheels were 0.71 m × 0.31 m.

Based on the vehicle load spectrum shown in Table 8, a command stream that let the front axle of the vehicle travel from one end of the bridge deck until the rear axle leaves the other end of the bridge in turn were written by ANSYS APDL. Each load step was recorded to obtain the stress-time history of the concerned point, as shown in Figure 12.

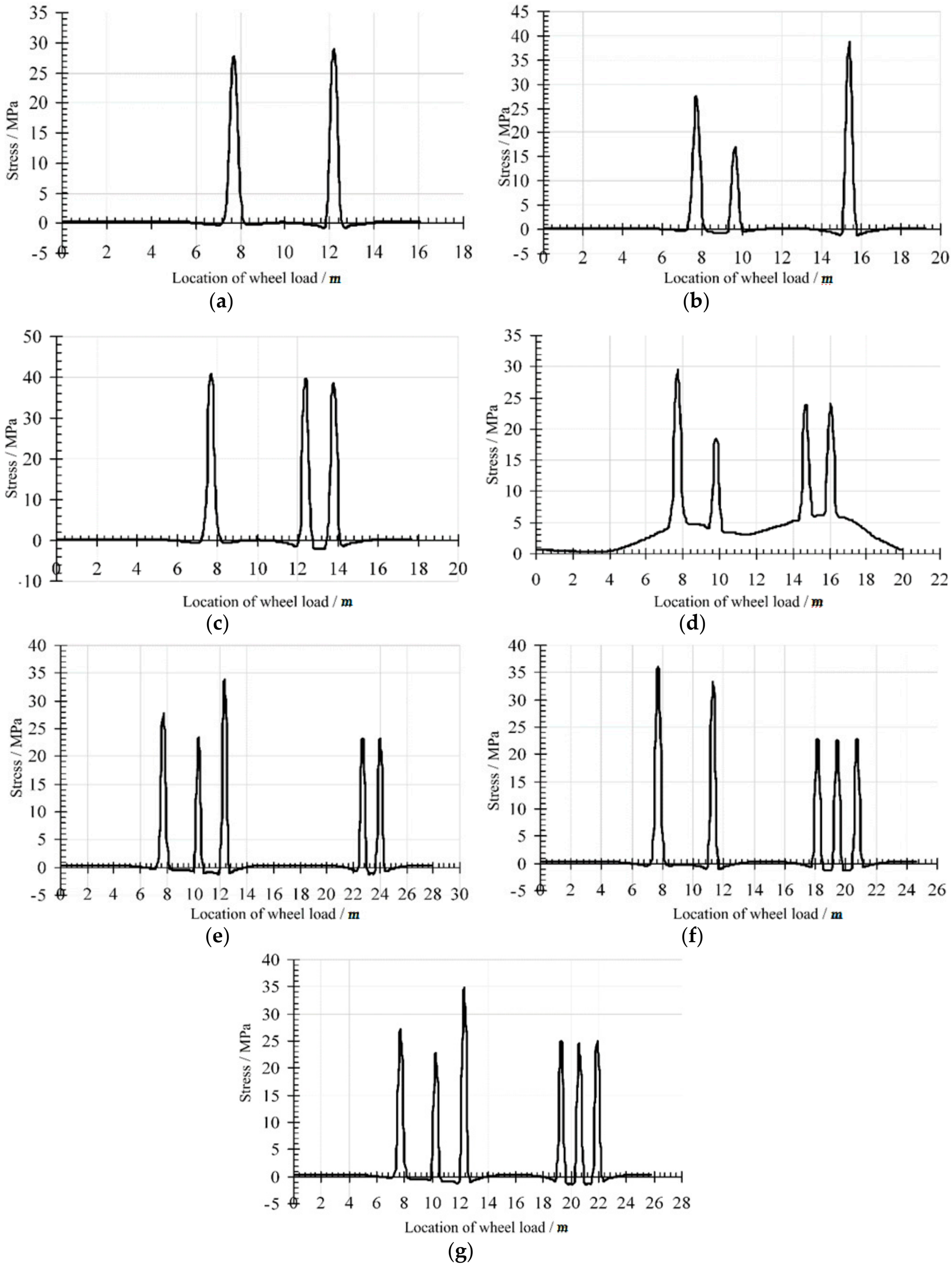

Figure 12. The stress-time curve of concerned point by various vehicles load: (**a**) Vehicle model V1; (**b**) Vehicle model V2; (**c**) Vehicle model V3; (**d**) Vehicle model V4; (**e**) Vehicle model V5; (**f**) Vehicle model V6; and (**g**) Vehicle model V7.

According to the actual vehicle survey data, the stress history of the concerned point was analyzed by the rain flow counting method, and the maximum stress amplitude was 38.29 MPa. The stress amplitude range (0–40 MPa) was divided into eight levels equally [31], and the corresponding number of cycles of the concerned point in one year of each stress level was calculated, as shown in Table 11.

Table 11. Stress amplitude and the corresponding number of cycles (one year).

Stress Level	Stress Amplitude/MPa	Number of Cycles
1	0–5	498,915
2	5–10	0
3	10–15	838,642
4	15–20	183,148
5	20–25	1,139,528
6	25–30	997,920
7	30–35	339,727
8	35–40	78,374
Total		4,076,254

4. Fatigue Life Assessment of the Concerned Point

In order to evaluate the fatigue life of the details of the deck plate at the weld joint with U-rib and diaphragm, the $\Delta\sigma$-N curve obtained from the fatigue test was extended to the long life range according to the Eurocode 3 [32], and then the $\Delta\sigma$-N curve that met the requirement of the fatigue design of the details could be obtained, as shown in Figure 13.

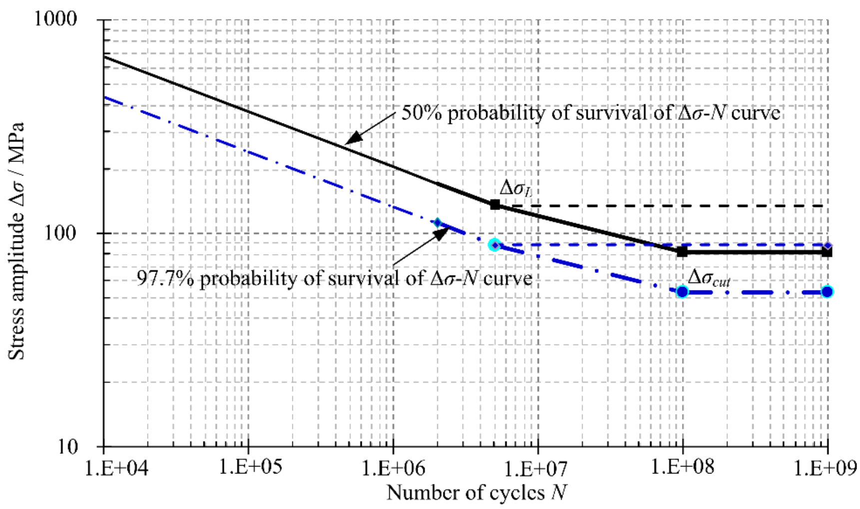

Figure 13. The extended $\Delta\sigma$-N curves.

According to the Eurocode 3, the detail category used to designate a particular fatigue strength curve corresponded to the reference value (in N/mm^2) of the fatigue strength at two million cycles, the constant amplitude fatigue limit corresponded to the fatigue strength for five million cycles, and the cut-off limit corresponded to the fatigue strength for 100 million cycles. According to the test result, when the probability of survival was 50%, the constant amplitude fatigue limit ($N = 5 \times 10^6$) of the detail of the weld joint was $\Delta\sigma_{L50\%} = 135.71$ MPa, and the cut-off limit ($N = 10^8$) was $\Delta\sigma_{\mathrm{cut}50\%} = 81.50$ MPa. The maximum stress amplitude of the detail was 38.29 MPa, less than the cut-off limit. When the probability of survival was 97.7%, the constant amplitude fatigue limit ($N = 5 \times 10^6$) of the detail was $\Delta\sigma_{L97.7\%} = 88.43$ MPa, and the cut-off limit ($N = 10^8$) was $\Delta\sigma_{\mathrm{cut}97.7\%} = 53.11$ MPa.

The maximum stress amplitude of the detail was 38.29 MPa, less than the cut-off limit. As the maximum stress amplitude of the detail was less than the cut-off limit, it was considered that there was no fatigue damage of the details of the weld joint.

If the maximum stress amplitude of the detail was more than the constant amplitude fatigue limit, combining with the Miner's Rule and Eurocode 3 [32], the amount of fatigue damage of the weld detail of the structure at 50% probability of survival could be calculated as shown in Equation (4), and at 97.7% probability of survival could be calculated as shown in Equation (5):

$$\begin{cases} D_i = n_i/N_i = n_i/(5\times10^6)(\frac{135.71}{\Delta\sigma_i})^{3.876}, & 135.71 \le \Delta\sigma_i \\ D_i = n_i/N_i = n_i/(5\times10^6)(\frac{135.71}{\Delta\sigma_i})^{5.876}, & 81.50 \le \Delta\sigma_i < 135.71 \\ D_i = n_i/N_i = 0, & \Delta\sigma_i \le 81.50 \end{cases}, \quad (4)$$

$$\begin{cases} D_i = n_i/N_i = n_i/(5\times10^6)(\frac{88.43}{\Delta\sigma_i})^{3.876}, & 88.43 \le \Delta\sigma_i \\ D_i = n_i/N_i = n_i/(5\times10^6)(\frac{88.43}{\Delta\sigma_i})^{5.876}, & 53.11 \le \Delta\sigma_i < 88.43 \\ D_i = n_i/N_i = 0, & \Delta\sigma_i \le 53.11 \end{cases}, \quad (5)$$

The total amount of fatigue damage of the details of the structure could also be calculated as shown in Equation (6) [33]:

$$D = \sum D_i = \sum \frac{n_i}{N_i}, \quad (6)$$

where D is the total amount of fatigue damage, $\Delta\sigma_i$ is the i-th stress amplitude, N_i is the total number of cycles of the i-th stress amplitude, n_i is the number of cycles of the i-th stress amplitude, and i = 1, 2, 3, 4, 5, ...

5. Conclusions

This paper focused on the fatigue strength of the weld joint of the deck plate at its weld joint with U-rib and diaphragm in an orthotropic steel bridge deck, researched the mechanical properties of the steel plate and the microstructure of the welded joint, then designed the fatigue specimens of the deck plate and did the fatigue test. The fatigue test results showed that the fatigue life would be improved significantly when the surface of the specimen was polished and smoothed. The test results also showed that the initiation life of the crack in the weld detail was longer than the crack propagation life. The $\Delta\sigma$-N curves and stress amplitudes of the deck plate at its weld joint with U rib and diaphragm under a different probability of survival were obtained. After extending the $\Delta\sigma$-N curves to the long life range, the extended $\Delta\sigma$-N curve and the amount of fatigue damage calculation equation that met the requirement of the fatigue design of the detail was proposed, and the cut-off limit under the 50% and 97.7% probability of survival were 81.50 MPa and 53.11 MPa, respectively.

This paper also established a simplified finite element model of the steel box girder section, determined the concerned point where the fatigue cracks easily generated, selected a reasonable loading process and the impact coefficient, and calculated the stress amplitude of the details of the weld joint using the actual vehicle load spectrum. The calculation result showed that the maximum stress amplitude of the concerned point was 38.29 MPa, less than the cut-off limit. It meant that the fatigue strength of the details of the weld joint met the requirement of the fatigue design.

Author Contributions: Methodology, Y.C.; software, Y.C. and D.L.; supervision, P.L.; writing—original draft preparation, Y.C.; writing—review and editing, Y.C. and P.L.

Funding: This research was funded by the Fundamental Research Funds for the Central Universities of Chang'an University, grant number 310825171012 and 300102259302.

Conflicts of Interest: The authors declare no conflict of interest.

References

1. Ya, S.; Yamada, K.; Shikawa, T. Fatigue evaluation of rib-to-deck welded joints of orthotropic steel bridge deck. *J. Bridge Eng.* **2013**, *18*, 492–499. [CrossRef]
2. Oh, C.K.; Hong, K.J.; Bae, D.; Do, H.; Han, T. Analytical and experimental studies on optimal details of orthotropic steel decks for long span bridges. *Int. J. Steel Struct.* **2011**, *11*, 227–234. [CrossRef]
3. Fu, Z.; Ji, B.; Zhang, C.; Li, D. Experimental study on the fatigue performance of roof and U-rib welds of orthotropic steel bridge decks. *KSCE J Civ. Eng.* **2018**, *22*, 270–278. [CrossRef]
4. Freitas, S.T.D.; Kolstein, H.; Bijlaard, F. Fatigue behavior of bonded and sandwich systems for strengthening orthotropic bridge decks. *Compos. Struct.* **2013**, *97*, 117–128. [CrossRef]
5. Kainuma, S.; Ahn, J.H.; Jeong, Y.S.; Sugiyama, H.; Iwasaki, M. Evaluation of structural responses on artificial fatigue crack for bulb rib orthotropic deck. *Adv. Struct. Eng.* **2016**, *18*, 1355–1369. [CrossRef]
6. Bocchieri, W.J.; Fisher, J.W. *Williamsburg Bridge Replacement Orthotropic Deck as-Built Fatigue Test*; ATLSS Report; Lehigh University: Bethlehem, PA, USA, 1998.
7. Connor, R.J.; Richards, S.O.; Fisher, J.W. Long-term remote monitoring of prototype orthotropic deck panels on the Bronx-Whitestone Bridge for fatigue evaluation. In *Recent Developments in Bridge Engineering*; Swets &Zeitlinger B.V.: Lisse, The Netherlands, 2003; pp. 257–268.
8. Cullimore, M.S.G.; Webber, D. Analysis of heavy girder bridge fatigue failures. *Eng. Fail. Anal.* **2000**, *7*, 145–168. [CrossRef]
9. Choi, D.H.; Choi, H.Y.; Choi, J.H. The effect of diaphragm inside trough rib on fatigue behavior of trough rib and cross beam connections in orthotropic steel decks. *J. Korean Soc. Steel Constr.* **2000**, *23*, 239–250.
10. Nguyen, H.T.; Chu, Q.T.; Kim, S.E. Fatigue analysis of a pre-fabricated orthotropic steel deck for light-weight vehicles. *J. Constr. Steel Res.* **2011**, *67*, 647–655. [CrossRef]
11. Battista, R.C.; Pfeil, M.S.; Carvalho, E.M.L. Fatigue life estimates for a slender orthotropic steel deck. *J. Constr. Steel Res.* **2008**, *64*, 134–143. [CrossRef]
12. Cui, C.; Zhang, Q.H.; Luo, Y.; Hao, H.; Li, J. Fatigue reliability evaluation of deck-to-rib welded joints in OSD considering stochastic traffic load and welding residual stress. *Int. J. Fatigue* **2018**, *111*, 151–160. [CrossRef]
13. Farreras-Alcover, I.; Chryssanthopoulos, M.K.; Andersen, J.E. Data-based models for fatigue reliability of orthotropic steel bridge decks based on temperature, traffic and strain monitoring. *Int. J. Fatigue* **2017**, *95*, 104–119. [CrossRef]
14. Kainuma, S.; Jeong, Y.S.; Ahn, J.H.; Yamagami, T.; Tsukamoto, S. Behavior and stress of orthotropic deck with bulb rib by surface corrosion. *J. Constr. Steel Res.* **2015**, *113*, 135–145. [CrossRef]
15. Wolchuk, R. Lessons from weld cracks in orthotropic decks on three European bridges. *J. Struct. Eng.* **1990**, *116*, 75–84. [CrossRef]
16. Tsakopoulos, P.A.; Fisher, J.W. Full-scale fatigue tests of steel orthotropic deck panel for the Bronx—Whitestone Bridge rehabilitation. *Bridge Struct.* **2005**, *1*, 55–66. [CrossRef]
17. Connor, R.J.; Fisher, J.W. Consistent approach to calculating stresses for fatigue design of welded rib-to-web connections in steel orthotropic bridge decks. *J. Bridge Eng.* **2006**, *11*, 517–525. [CrossRef]
18. Maljaars, J.; Bonet, E.; Pijpers, R.J.M. Fatigue resistance of the deck plate in steel orthotropic deck structures. *Eng. Fract. Mech.* **2018**, *201*, 214–228. [CrossRef]
19. Xiao, Z.G.; Yamada, K.; Ya, S.; Zhao, X.L. Stress analyses and fatigue evaluation of rib-to-deck joints in steel orthotropic decks. *Int. J. Fatigue* **2008**, *30*, 1387–1397. [CrossRef]
20. Kainuma, S.; Yang, M.Y.; Jeong, Y.S.; Inokuchi, S.; Kawabata, A.; Uchida, D. Experimental investigation for structural parameter effects on fatigue behavior of rib-to-deck welded joints in orthotropic steel decks. *Eng. Fail. Anal.* **2017**, *79*, 520–537. [CrossRef]
21. Kainuma, S.; Yang, M.Y.; Jeong, Y.S.; Inokuchi, S.; Kawabata, A.; Uchida, D. Fatigue Behavior Investigation and Stress Analysis for Rib-to-Deck Welded Joints in Orthotropic Steel Decks. *Int. J. Steel Struct.* **2018**, *18*, 512–527. [CrossRef]
22. Heng, J.; Zheng, K.; Gou, C.; Zhang, Y.; Bao, Y. Fatigue performance of rib-to-deck joints in orthotropic steel decks with thickened edge U-ribs. *J. Bridge Eng.* **2017**, *22*, 04017059. [CrossRef]
23. Yu, B.; Qiu, H.X.; Wang, H.; Guo, T. Experimental research on fatigue behavior and damage development of welded conformation of orthotropic steel bridge deck. *J. Highway Transp. Res. Dev.* **2009**, *26*, 64–69.

24. Luo, P.J.; Zhang, Q.H.; Bao, Y.; Zhou, A.X. Fatigue evaluation of rib-to-deck welded joint using averaged strain energy density method. *Eng. Struct.* **2018**, *177*, 682–694. [CrossRef]
25. Zeng, Z.B. Classification and reasons of typical fatigue cracks in orthotropic steel deck. *Steel Constr.* **2011**, *26*, 9–16.
26. ISO. Metallic materials-tensile testing, Part 1: Method of test at room temperature. *Int. Organiz. Stand.* **2016**, 6892-1.
27. TB 10002.2. *Code for Design on Steel Structure of Railway Bridge*; China Railway Publishing House: Beijing, China, 2005.
28. GB/T 10045-2001. *Carbon Steel Flux Cored Electrodes for Arc Welding*; Standards Press of China: Beijing, China, 2001.
29. Zhou, Y.B. Crack Study and Local Fatigue Analysis of Orthotropic Steel Decks on Bridges. Master's Thesis, Tsinghua University, Beijing, China, 2010.
30. AASHTO. *AASHTO LRFD Bridge Design Specifications*; American Association of State Highway and Transportation Officials: Washington, DC, USA, 2007.
31. Sonsino, C.M. Fatigue testing under variable amplitude loading. *Int. J. Fatigue* **2007**, *29*, 1080–1089. [CrossRef]
32. EN. *Eurocode 3: Design of Steel Structures, Part 1–9: Fatigue Strength of Steel Structures*; European Committee for Standardization: Brussels, Belgium, 2003.
33. Lee, Y.L.; Pan, J.; Hathaway, R.; Barkey, M. *Fatigue Testing and Analysis: Theory and Practice (Vol. 13)*; Butterworth-Heinemann: Burlington, MA, USA, 2005.